# Effect of Repetition Rate on Ultrashort Pulse Laser Propagation and Energy Deposition

Jessica Peña\*a,b, Eric W. Rosenthal<sup>c</sup>, Alexander Englesbe<sup>a</sup>, Joshua Isaacs<sup>a</sup>, Michael Helle<sup>a</sup>, Joseph Peñano<sup>a</sup>

<sup>a</sup>Plasma Physics Division, U.S. Naval Research Laboratory, 4555 Overlook Avenue SW,
Washington DC 20375, USA;
<sup>b</sup>National Science Foundation MPS-Ascend Postdoctoral Fellowship,
2415 Eisenhower Avenue, Alexandria VA 22314, USA;
<sup>c</sup>Tactical Electronic Warfare Division, U.S.
Naval Research Laboratory, 4555 Overlook Avenue SW, Washington DC 20375, USA

#### **ABSTRACT**

Modern USPL (ultra short pulse laser) development is trending towards higher repetition rates and higher average power systems. High peak power, low repetition rate USPLs have long been used to generate laser filaments, which consist of a plasma channel and region of focused high intensity propagation. Filamentation leads to heat deposition in the air from linear and nonlinear effects, producing a gas density depression that persists over hydrodynamic timescales (milliseconds). This is long after the femtosecond pulse has passed. In the "single-shot" (~10 Hz) regime of filamentation, the time between pulses allows the air density to return to equilibrium before the next pulse arrives. Prior work has experimentally measured the single shot gas density depression via interferometry and demonstrated that high repetition rate filamentation leads to deflection of subsequent pulses due to residual heating from the prior pulses and spatially examines USPL thermal blooming as a function of laser repetition rate. Residual heating effects between pulses are demonstrated through measurements of the energy deposition by the laser filament. The temporally and spatially resolved energy deposition is extracted from interferometric measurements of the phase shift due to the gas density depression. Comparison is made between experimentation and modeling, as well as verification of past results. This work demonstrates how atmospheric propagation of modern high average power, high repetition rate USPL pulses differ from traditional single shot USPL systems.

Keywords: Ultrashort Pulse Lasers, Thermal Blooming, Filamentation

#### 1. INTRODUCTION

Laser filamentation is a well-known phenomenon in which the balance between nonlinear self-focusing of an intense laser pulse and plasma defocusing produces a plasma channel with clamped electron density<sup>4</sup> (10<sup>16</sup> cm<sup>-3</sup>) and propagation region with clamped laser intensity<sup>5</sup> (~10<sup>13</sup> W/cm<sup>2</sup>). Much of the body of prior work studies "single shot" filamentation, meaning the lasers used had low repetition rates and the time between pulses was sufficiently long for the air to return to equilibrium<sup>6, 7</sup>. Modern USPL technology is trending towards higher repetition rates, as 1 kHz lasers are now common technology and new sources are reaching 100 kHz<sup>8</sup>. As the repetition rate increases, a laser pulse can no longer be considered individually, but instead propagates through a medium influenced by the preceding pulse. Here, we present measurements of the filament-induced density depression at different laser repetition rates. Comparison with modeling indicates the need for an improved molecular response model to accurately simulate the effect of combining high average power with high peak power during laser propagation.

# 1.1 Energy Deposition via Filamentation

Laser energy is depleted from the optical field and deposited into the propagation medium as heat during the filamentation process through several mechanisms, including linear absorption, ionization, rotational Raman excitation, and inverse Bremsstrahlung<sup>1</sup>. Rotational Raman excitation is only relevant when the pulse is propagating through a molecular medium, like air. Laser energy lost to ionization and rotational excitations are deposited as heat in the atmosphere. The plasma lifetime is on the timescale of several nanoseconds<sup>9</sup>, and the timescale for rotationally excited molecules to collisionally decohere is ~100 ps<sup>10</sup>. These timescales are much less than the acoustic response timescale of the gas, which is typically several hundred nanoseconds<sup>1</sup>. Therefore, the impulsive nature of the on-axis pressure increase will drive an outwardly

\*jessica.pena.ctr@nrl.navy.mil

propagating acoustic wave<sup>11</sup> that carries the deposited energy away. The acoustic wave leaves behind a long-lived gas density depression that dissipates on a millisecond timescale via thermal diffusion. Prior work has characterized this density depression for single shot filamentation<sup>1, 12</sup>. Once the repetition rate approaches a hydrodynamic timescale between pulses (i.e. kHz rep rates), each pulse will interact with the density depression left behind by the preceding pulse. Several studies indicate that high repetition rates lead to beam deflection<sup>2</sup> and other cumulative effects<sup>3, 12</sup>. This work seeks to experimentally observe the "turn-on" of cumulative effects and motivates the need for a more robust rotational excitation model to fully capture such effects

# 2. MODELING AND DIAGNOSTIC TECHNIQUES

Higher repetition rates and cumulative effects are experimentally measured using interferometric techniques. Comparison is made to modeling for the single shot data. Both the modeling and experimental diagnostic use the change in refractive index induced by the density depression to determine the energy deposited by the laser pulse into the gas.

## 2.1 Modeling the Energy Deposition

Simulations of the pulse propagation, filament formation, and evolution of the density depression were carried out. The pulse propagation and filament formation are simulated using NRL's PyCAP (Python Code for Atmospheric Propagation)<sup>2</sup>. To calculate the thermal refractive index perturbation, the laser energy lost to different absorption processes first must be determined. The absorption coefficients due to ionization and rotational Raman excitation are derived by Isaacs et. al. <sup>2</sup> for an ultrashort laser pulse. The fluence loss due to ionization is evaluated based on the electron density and energy density directly behind the laser pulse, i.e. before recombination and relaxation. The rotational Raman excitation is modeled as an effective two-level system centered around the transition from J=8 to J=6, which dominates for pulse durations less than 1 ps and for a central wavelength  $\lambda_0$ =800 nm.

The relative effect of absorption due to ionization and rotational Raman excitation was demonstrated to depend on the pulse duration and energy<sup>2</sup>. At lower pulse energies (3 mJ), longer pulse durations ( $\tau > 200 \, fs$ ) result in stronger absorption and heat deposition from rotational Raman excitation than from ionization. Ionization loss dominates for pulse durations less than 100 fs. As the pulse energy is increased to 10 mJ, the pulse duration dependence is pushed out to longer durations. Ionization dominates for  $\tau < 300 \, fs$  and rotational Raman dominates for  $\tau > 1 \, ps$ . This strong dependence on pulse parameters motivates the need for precise experimental pulse characterization to ensure an accurate comparison to the model.

A region of elevated temperature results from fluence loss and absorption. This energy is then carried away by an acoustic wave, leaving behind a region of depressed density. Calculation of the refractive index change due to this depression is calculated for an isobaric condition, i.e. after the transit time of the acoustic wave but before the timescale for thermal dissipation<sup>2</sup>. Simulation of the refractive index change due to thermal dissipation provides a direct comparison to experimental interferometric measurements of the density depression.

## 2.2 Experimental Measurement of Energy Deposition

Interferometric techniques are used to experimentally measure the density depression. The experiment setup is shown in Figure 1, and is based on an experiment design used in prior studies of the density depression<sup>1</sup>. The pump pulse was generated by a Ti:Sapphire ultra-short pulse laser (USPL) with a central wavelength of 800 nm, a repetition rate of 1 kHz, a 45 fs transform limited pulse duration, and tunable energy. For this experiment, the energy was varied between 1-3 mJ and the FWHM beam diameter was varied from 5 to 9 mm using an iris. The repetition rate is controllable from 10 to 1000 Hz using a Thorlabs Optical Chopper system. The f-number varied between f/320 and f/580 as an iris was closed down. The pump generated a ~30 cm filament. The probe laser (Thorlabs NPL52C) produces 10 ns pulses at  $\lambda = 520$  nm. A dichroic mirror was used to co-propagate the pump and probe. After interacting with the filament, the probe laser was split off from the pump using a second dichroic mirror before entering a folded wavefront interferometer, which was used to measure the phase shift induced by the density depression existing long after the USPL propagates away. Timing between the pump and the probe lasers was controllable using a Stanford Research Systems DG645, enabling time resolved measurements of the density depression.

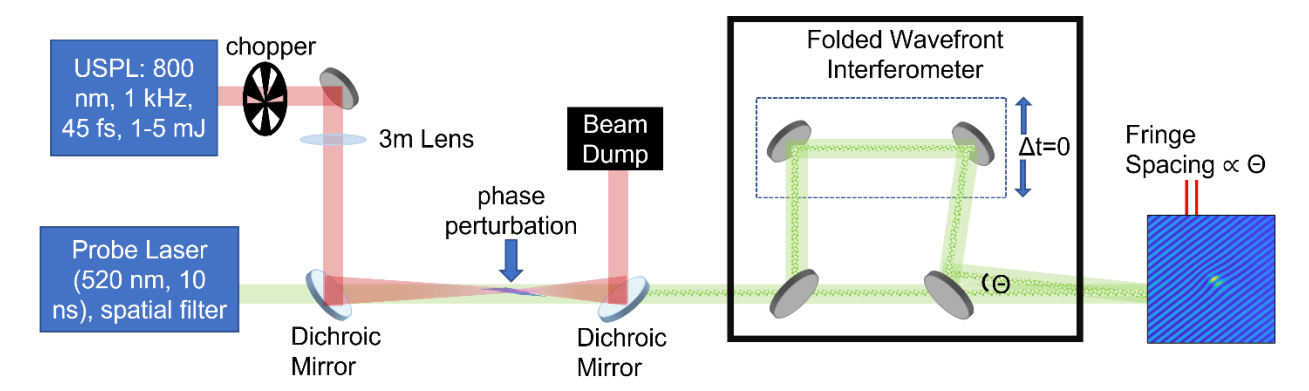


Figure 1: Experiment setup. The 800 nm USPL pump beam generates filaments at a repetition rate controlled by the chopper. The 520 nm probe laser co-propagates with the pump. The delay between the pump and probe is set by a delay generator.

The phase shift was extracted from the interferogram using well-known methods<sup>13</sup>. Many prior studies have used a copropagating or small-angle interferometric technique to calculate energy deposition<sup>1, 3</sup> and plasma electron density<sup>9, 14</sup>. However, this study utilized an improved high precision background subtraction routine, leading to phase noise on the order of a few milliradians. Figure 2 demonstrates the steps involved in the high precision background subtraction routine. The signal and background phase, obtained from interferograms, are shown in panels a and b respectively. Subtracting the background phase from the signal phase results in panel c. At this point, the energy deposition can be calculated, but the phase noise is still tens of milliradians. A further improvement in experimental phase noise is achieved by applying a low-spatial-frequency fit to the part of the image not containing our desired signal. A fifth-order polynomial surface is fit to the points outside of the red circle (Fig. 2.d), effectively excluding the density depression from the fit while interpolating the background phase noise over the entire image. By subtracting this fit from the initial phase (Fig. 2.c), a much flatter background is obtained. A surface plot is shown in Fig. 2.e, and the final retrieved phase is shown in Fig. 2.f, both of which demonstrate background phase noise on the order of a few milliradians. Using this background subtraction routine enables detection of lower amplitude signals enabling more precise measurements.

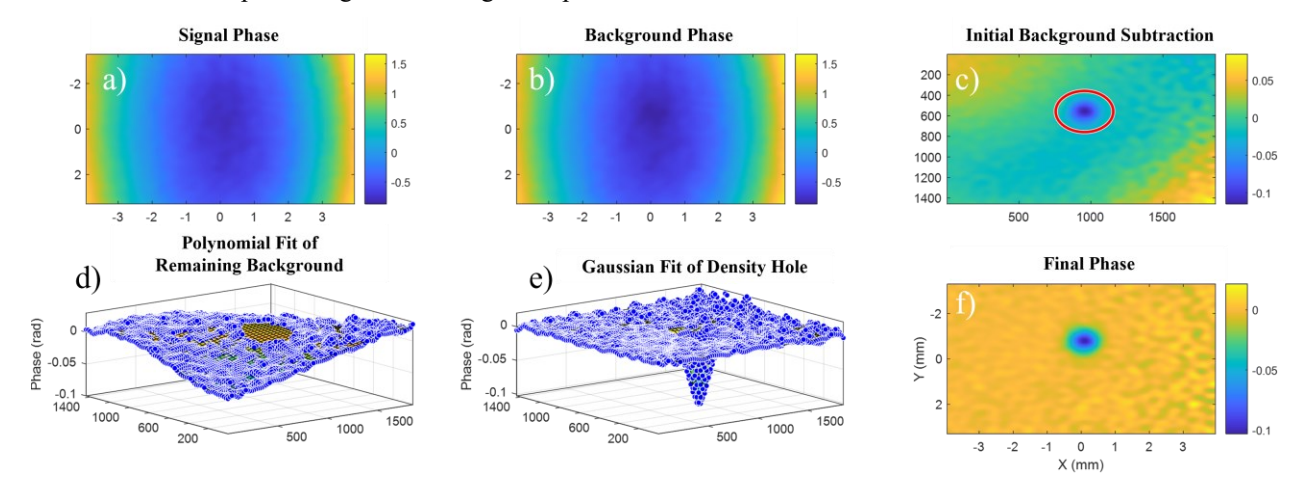


Figure 2: Example illustrating the high precision background subtraction routine and calculation of energy deposition.

Once the phase has been retrieved and the background subtracted, the energy deposition is calculated. The calculation follows that described in prior work<sup>1</sup>. The phase can be related to a change in refractive index by  $\Delta n = \frac{\Delta \phi}{k_0 L}$ , where  $k_0$  is the wavenumber and L is the filament length. A map of the energy deposition, similar to the phase map in Fig. 2.f, can then be obtained through  $E_{dep} = \frac{-c_v T_0 \rho_0 L}{n_0 - 1} \Delta n$ . Here,  $c_v$  is the specific heat at constant volume,  $T_0$  is the ambient temperature,  $\rho_0$  is the air density, and  $n_0 - 1$  is the refractivity. Notably, the filament length parameter drops out of the equation when mapping directly from phase to energy deposition. Integration over the filament length occurs as the pulse physically traverses the length of the filament and does not need to be separately measured to obtain an accurate

measurement of energy deposition. Integrating over the transversely resolved energy deposition results in a scalar total deposited energy.

#### 3. RESULTS

Experiments were performed for the single shot regime (~10 Hz) and in incremental repetition rates up to 1 kHz. Cumulative effects were found to begin at a 250 Hz repetition rate. The pulse energy was varied from 0.6 to 2.0 mJ in the single shot regime. Comparisons between the single shot data and modeling are made. The need for an improved molecular response model is apparent when comparing the model to this dataset and prior experimental work.

#### 3.1 Repetition Rate Scaling

Experiments confirm the effect of scaling repetition rate. Prior work has extensively studied the energy deposition in the single shot regime<sup>1</sup> and has shown the onset of cumulative effects on the filament location at repetition rates above 250 Hz<sup>12</sup>. The results presented here provide a comprehensive repetition rate scaling from 10 Hz to 1 kHz, and comparison to prior work verifies the repeatability and accuracy of the experimental results. This is necessary to ensure discrepancies with the model are not a result of experimental inaccuracies.

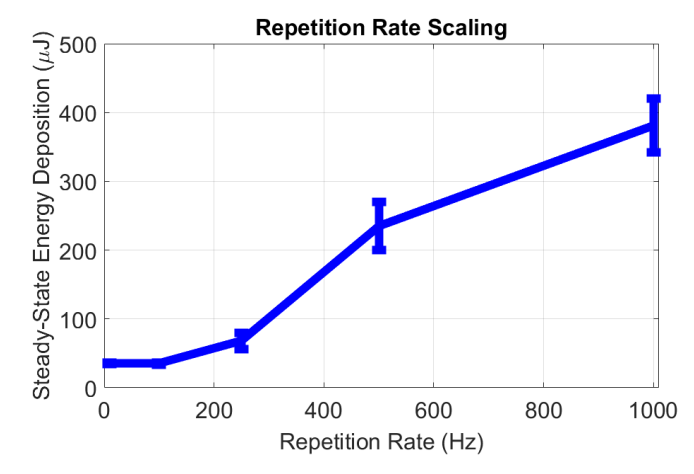


Figure 3: Steady state deposited energy at laser repetition rates from 10 to 1000 Hz averaged over data taken with probe delays of 30, 100, 500, and 900 µs.

The measured energy deposition at all repetition rates is shown in Figure 3. For this data, the energy per pulse remained constant at 2 mJ, the beam FWHM diameter was 7 mm, and the beam was focused using an f/414 geometry. Data was taken for probe delays from 30 to 900  $\mu$ s, which are all late enough that the acoustic wave has long since propagated away and the depth of the density hole is stable. The data shown is an average of the four measured probe delays. The density hole itself is a good measure of deposited energy for single shot filaments. For repetition rates at and above 250 Hz, cumulative effects are evident and impact the interferometric measurement. Below 250 Hz, the energy deposition is consistently measured to be ~35  $\mu$ J. Prior work with similar laser parameters found an energy deposition of ~25  $\mu$ J for a 2 mJ initial pulse energy<sup>1</sup>. The modestly increased energy deposition value in this study is likely due to a slight difference in initial focusing conditions, with an f/414 geometry used in this work while prior work used an f/600 focusing geometry<sup>1</sup>. The f-number has been demonstrated to have a significant effect on plasma properties<sup>9</sup>, including the energy deposition <sup>15</sup>. Above 250 Hz, we see an integrated density hole that steadily increases with repetition rate.

#### 3.2 Comparison to Simulations

Prior modeling work has overestimated various experimentally measured long-timescale gas hydrodynamic behaviors by 40-400%<sup>2</sup>. To accurately model high repetition rate effects, agreement must first be achieved at the single shot level. To this end, Figure 4 compares the experiment and modeling. In this case, the laser repetition rate was kept constant at 10 Hz, the beam FWHM diameter was maintained at 5 mm, and the energy was incrementally varied from 0.6 to 1.6 mJ. The PyCAP model was run using the exact same parameters. An experimentally measured beam profile was used as the simulation input beam to eliminate discrepancies based on a non-ideal experimental beam profile. Variations in the beam profile were found to have little effect on the simulated energy deposition. In Figure 4, the orange line indicates simulation results and the blue data points are experimental. At each laser pulse energy, the simulation overestimates the magnitude

of energy deposition compared to the measurements. At the lowest pulse energy, the values are within a factor of two, but as the pulse energy increases the difference between the experimentally retrieved and simulated energy deposition is nearly four times. Ongoing work is investigating whether the assumptions regarding the transition from the isovolumetric to isobaric regime cause an underestimation of the experimental energy deposition. However, this would likely result in a ~30% mismatch and would not account for a four times discrepancy between the experiment and simulation. It has been shown that rotational heating may account for 30-60% of the total energy deposition <sup>15</sup>. This motivated a second run of the simulation with only the ionization model (gray data points). This matched the experiment at the lowest pulse energy and deviated less from experimental values, but still demonstrates a factor of two mismatch.

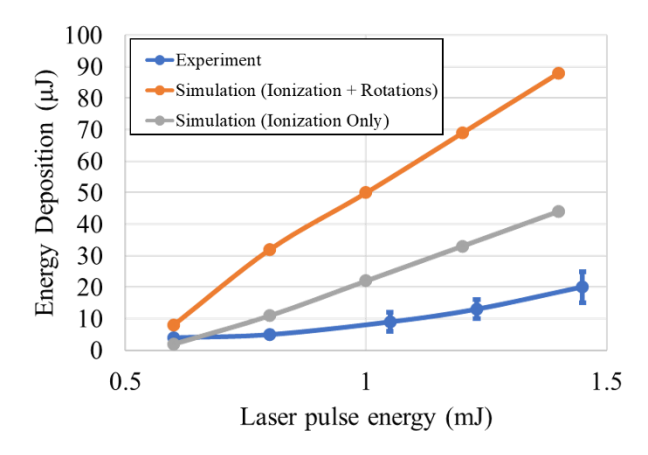


Figure 4: Comparison of the experimentally measured (blue) energy deposition values to the simulated values with ionization and rotational excitation models (orange) and simulations with only ionization considered (grey).

Additionally, the curvature of the trends does not match between the experiment and simulation. It would be expected that the energy deposition would be proportional to the square of the intensity,  $E_{dep} \propto I^2$  because rotational excitation is a two-photon process. The experimental data exhibits this trend, while the orange curve illustrating simulation results with ionization and rotations has the opposite concavity. In the gray data points, where rotations were removed from the simulation, the curve is nearly linear, indicating that the rotational model was responsible for the curvature in the full simulation. While the rotational model alone is likely not the sole cause of the discrepancy between experiment and simulation, it is worth further investigation. We are currently performing experiments with monatomic gases in order to isolate the rotational absorption experienced in air, thus providing a strong comparison point for the model.

#### 4. CONCLUSIONS

This work experimentally demonstrates the effect of increasing the average power of a high peak power USPL, identifying a turn-on of cumulative effects at 250 Hz. This aligns with prior experimental studies, validating the repeatability and accuracy of the experimental measurements. Verification was necessary as significant discrepancy was observed between the model and experiment. This discrepancy likely arises from the need for a more robust rotational excitation model, which must be amended to accurately capture high repetition rate effects. Ongoing and future research efforts are investigating the validity of this claim by repeating measurements in an atomic gas, where there is no rotational excitation.

## **ACKNOWLEDGEMENTS**

J. Peña is supported by the National Science Foundation MPS-Ascend Postdoctoral Research Fellowship under Grant No. 2213242. This work is supported by the Office of Naval Research.

#### REFERENCES

- [1] Rosenthal, E. W., Jhajj, N., Larkin, I., Zahedpour, S., Wahlstrand, J. K. and Milchberg, H. M., "Energy deposition of single femtosecond filaments in the atmosphere," *Optics Letters* **41**(16), 3908-3911 (2016). https://doi.org/10.1364/ol.41.003908.
- [2] Isaacs, J., Hafizi, B., Johnson, L. A., Rosenthal, E. W., Mrini, L. and Peñano, J., "Modeling the propagation of a high-average-power train of ultrashort laser pulses," *Opt. Express* **30**(13), 22306-22320 (2022). https://doi.org/10.1364/OE.443989.
- [3] Jhajj, N., Rosenthal, E. W., Birnbaum, R., Wahlstrand, J. K. and Milchberg, H. M., "Demonstration of long-lived high-power optical waveguides in air," *Physical Review X* 4(1), (2014). https://doi.org/10.1103/PhysRevX.4.011027.
- [4] La Fontaine, B. et al., "Filamentation of ultrashort pulse laser beams resulting from their propagation over long distances in air," *Physics of Plasmas* 6(5), 1615-1621 (1999). https://doi.org/10.1063/1.873715.
- [5] Kasparian, J., Sauerbrey, R. and Chin, S. L., "The critical laser intensity of self-guided light filaments in air," Appl. Phys. B-Lasers Opt. 71(6), 877-879 (2000). https://doi.org/10.1007/s003400000463.
- [6] Chin, S. L. et al., "Advances in intense femtosecond laser filamentation in air," Laser Phys. 22(1), 1-53 (2012). https://doi.org/10.1134/s1054660x11190054.
- [7] Couairon, A. and Mysyrowicz, A., "Femtosecond filamentation in transparent media," *Phys. Rep.-Rev. Sec. Phys. Lett.* **441**(2-4), 47-189 (2007). https://doi.org/10.1016/j.physrep.2006.12.005.
- [8] Löscher, R. et al., "High-power sub-picosecond filamentation at 1.03 μm with high repetition rates between 10 and 100 khz," *APL Photonics* **8**(11), (2023). https://doi.org/10.1063/5.0175100.
- [9] Reyes, D., Baudelet, M., Richardson, M. and Fairchild, S. R., "Transition from linear- to nonlinear-focusing regime of laser filament plasma dynamics," *J. Appl. Phys.* **124**(5), 5 (2018). https://doi.org/10.1063/1.5027573.
- [10] Chen, Y. H., Varma, S., York, A. and Milchberg, H. M., "Single-shot, space- and time-resolved measurement of rotational wavepacket revivals in h2, d2, n2, o2, and n2o," *Opt. Express* 15(18), 11341-11357 (2007). https://doi.org/10.1364/OE.15.011341.
- [11] Wahlstrand, J. K., Jhajj, N., Rosenthal, E. W., Zahedpour, S. and Milchberg, H. M., "Direct imaging of the acoustic waves generated by femtosecond filaments in air," *Optics Letters* **39**(5), 1290-1293 (2014). https://doi.org/10.1364/ol.39.001290.
- [12] Cheng, Y. H., Wahlstrand, J. K., Jhajj, N. and Milchberg, H. M., "The effect of long timescale gas dynamics on femtosecond filamentation," *Opt. Express* **21**(4), 4740-4751 (2013). https://doi.org/10.1364/oe.21.004740.
- [13] Takeda, M., Ina, H. and Kobayashi, S., "Fourier-transform method of fringe-pattern analysis for computer-based topography and interferometry," *Journal of the Optical Society of America* **72**(1), 156-160 (1982). https://doi.org/10.1364/josa.72.000156.
- [14] Chen, Y. H., Varma, S., Antonsen, T. M. and Milchberg, H. M., "Direct measurement of the electron density of extended femtosecond laser pulse-induced filaments," *Physical Review Letters* **105**(21), (2010). https://doi.org/10.1103/PhysRevLett.105.215005.
- [15] Rosenthal, E. W., Palastro, J. P., Jhajj, N., Zahedpour, S., Wahlstrand, J. K. and Milchberg, H. M., "Sensitivity of propagation and energy deposition in femtosecond filamentation to the nonlinear refractive index," *Journal of Physics B-Atomic Molecular and Optical Physics* 48(9), (2015). https://doi.org/10.1088/0953-4075/48/9/094011.